

© 2019 IEEE. Personal use of this material is permitted. Permission from IEEE must be obtained for all other uses, in any current or future media, including reprinting/republishing this material for advertising or promotional purposes, creating new collective works, for resale or redistribution to servers or lists, or reuse of any copyrighted component of this work in other works.

This paper has been accepted for publication by

**IEEE Journal of Emerging and Selected Topics in Power Electronics.**

**DOI**

10.1109/JESTPE.2019.2949234

**Citation**

K. Surakitbovorn and J. Rivas-Davila, "A Method to Eliminate Discrete Inductors in a Class-E Inverter used in Wireless Power Transfer Applications," *IEEE J. Emerging and Selected Topics in Power Electronics*, in press.

**IEEE Xplore URL**

<https://ieeexplore.ieee.org/document/8882287>

More papers from Juan Rivas's group at Stanford University can be found here:

<http://superlab.stanford.edu/publications.html>

# A Method to Eliminate Discrete Inductors in a Class-E Inverter used in Wireless Power Transfer Applications

Kawin Surakitbovorn, *Student Member, IEEE*, and Juan M. Rivas-Davila, *Senior Member, IEEE*

**Abstract**—Wireless power transfer (WPT) systems have attracted tremendous attention over the past decade. Most compact, low power, WPT systems; however, utilize ferrites to shield and redirect the magnetic fields. Using magnetic material adds to the weight and system bulk. In this paper, we present a method to design WPT coils in which the leakage and magnetizing inductances are utilized in other parts of the circuit. This eliminates the need for discrete inductors commonly required in a resonant inverter, which additionally improves overall efficiency. Utilizing this technique, we demonstrate a small and light-weight 300 W 48-to-48 V WPT system with above 90% efficiency. We further propose a method to eliminate the input inductor required by the class-E inverter by utilizing the input power supply wires. Employing this method, we demonstrate a printed circuit board (PCB) based WPT circuit operating at 40.68 MHz, utilizing no discrete inductors other than the WPT coils themselves and weighing only seven grams. The following paper describes the design methodology as well as the procedure to eliminate discrete resonant inductors used in the implementation of our designs.

**Index Terms**—gallium nitride (GaN), inductor elimination, wireless power transfer (WPT), class-E amplifier, high frequency (HF), very high frequency (VHF), printed circuit board (PCB) based circuit.

## I. INTRODUCTION

The advancement of wireless power transfer (WPT) technology has opened up many new and exciting areas of application. Examples of recent WPT applications include wireless electric vehicles (EVs) charging [1]–[3], wearable electronics and sensors charging [4]–[6], mobile phone charging [7], [8], medical implants charging [9]–[11], and mid-air charging of drones [12]–[14]. For high power applications such as EVs charging, achieving high power transfer efficiency and low radiating EMI is of most importance. On the other hand, for many of the low to medium power applications, it is highly beneficial to have WPT systems that are small and lightweight, as well as have low design complexity and low part count, which allow them to be easily integrated into products, as well as be mass-produced.

Previously, the design of choice for WPT systems at tens to hundreds of watts of power has been a hard switched or quasi-resonant converter operating at low or medium frequencies (LF or MF). For instance, the Qi standard adopted by most mobile device manufacturers for wireless charging specifies frequency between 80–300 kHz [15]. While operating at these frequencies enable designs that are simple and small, resulting WPT systems are not necessarily lightweight. This is a result of using heavy magnetic materials, such as ferrites, which are

required in the implementation of the inductors operating at low switching frequencies.

In the design of WPT systems, although there is no limitation on what frequency can be used, regulations and EMI considerations can constrain the design space. In these applications, frequencies such as those in the industrial, scientific and medical (ISM) bands allotted specifically for non-telecommunication purposes are preferred. By operating at high or very high frequencies (HF or VHF), one can use air-cored inductors and eliminate the need for magnetic materials in inductive components. This helps to reduce the weight of the system significantly. Other benefits of operating at HF/VHF include the improvement of transient time and better load regulation. Moreover, operating at HF/VHF, especially with resonant soft-switching typologies, can also lead to simpler and lighter EMI filter designs, thanks to the smaller filter component size needed due to the higher frequency as well as the narrower EMI band due to the soft switching [16]–[18]. A number of studies have been done in the field of WPT at HF/VHF [19]–[23]. Nonetheless, in order to get the resonant soft switchings required for the HF/VHF operations, several air-core inductors are typically needed in the inverter circuit. This leads to voluminous designs that are not ideal for applications where having a small size is a priority. Attempts have been made to improve the size of the overall WPT system by integrating part of its magnetic components. Specifically, [24] proposes a method to model PCB-based WPT coils, [25] proposes a method to design the WPT coils so that they can be used as compensated inductors in an LCC system, and [26] proposes a method to combine the input inductors of a push-pull class-E circuit. However, to the best of our knowledge, there is not yet a system that has integrated all of its inductors into the WPT coils at HF/VHF while maintaining high efficiency.

In this paper, we present a method to eliminate the resonating inductors and improve the circuit's efficiency in a class-E resonant inverter used in WPT applications at HF/VHF. This is done by designing the WPT coils such that their leakage and the magnetizing inductances can be used as resonating inductors for the class-E power amplifiers, as well as part of the filtering and impedance matching stage. While this resonant inductors elimination method relies on knowing the precise value of the inductance matrix of the WPT coils, thus not suitable for applications where coils separation and orientation can vary, there are many applications in which

the power needs to be passed through a fixed gap where this technique is suitable. Section II will explain the proposed WPT coils design and the resonant inductor elimination method. Section III will demonstrate a design example where we utilize this technique to eliminate four out of six inductors from a push-pull class-E inverter at 13.56 MHz. By doing so, we were able to create a small and lightweight, regulated, 48 V to 48 V WPT system that is capable of transferring a maximum of 300 W of power over a 15 mm air gap with above 90% dc-to-dc efficiency.

Next, we further present a method to eliminate the input inductor required by the class-E inverter by utilizing the input power supply wires to replace its input inductor. Section IV will explain the criteria on the input power supply wires and the frequency selection such that this method can be utilized. Following this technique, section V will showcase the design of a simple “inductor-less” WPT circuit where no discrete inductor other than the two WPT coils is used. The circuit operates at 40.68 MHz and is capable of 20 W of power. By making the WPT coils out of the printed circuit board, the dc-dc system is remarkably low profile and lightweight, weighing at only seven grams.

## II. WPT COILS DESIGN & RESONANT INDUCTORS ELIMINATION TECHNIQUE

In traditional resonant WPT coils designs, both the leakage and the magnetizing inductance of the coils are canceled out by resonating capacitors, leaving the WPT coils as an ideal transformer [27]–[29]. To match the rectifier input impedance to the output impedance of the inverter, an extra matching network is typically used. Unfortunately, designing the WPT system this way does not lead to a reduction in the number of resonant inductors in the inverter circuit used to drive the WPT coils.

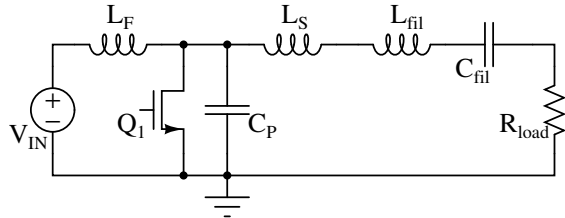


**Fig. 1:** The schematic of a class-E resonant inverter.

In this section, a new way of WPT coils design suitable for the WPT system utilizing a class-E inverter at HF/VHF is developed. Specifically, the WPT coils are designed such that their leakage ( $L_{leak}$ ) and magnetizing ( $L_{mag}$ ) inductance can be incorporated into the design of the class-E inverter and take the role of soft-switching inductor,  $L_S$ , and series filter inductor,  $L_{fil}$ , (shown in figure 1) as well as the matching network. By designing the WPT coils this way, we can completely eliminate the discrete resonant inductors on the inverter circuit. Since these discrete resonant inductors are typically lossy as well as bulky, this inductor elimination results in a significant improvement in both the system efficiency, as well

as the weight and the size of the system when compared to circuits designed with traditional WPT coils.

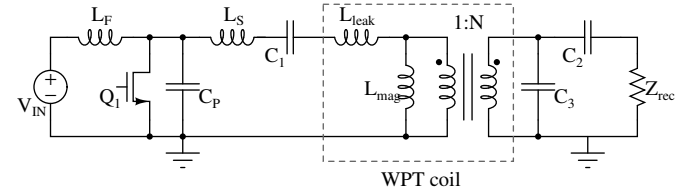


**Fig. 2:** The circuit diagram with WPT coils shown as a transformer in a cantilever model.

First, let us examine conceptually how this can be achieved. Shown in the circuit diagram in figure 2, the WPT coils are connected across the output of the class-E inverter and are modeled as a transformer in a cantilever model. A rectifier circuit is connected on the other side of the WPT coils and is modeled with a resistor,  $Z_{rec}$ . Furthermore, three extra capacitors,  $C_1$ ,  $C_2$  and  $C_3$ , are also shown. Their roles and values selection will be explained shortly.

As seen from this diagram,  $L_{leak}$  of the WPT coils is in series with  $L_S$  of the inverter.

This means that if  $L_{leak}$  of the WPT coils can be designed to have the value of  $L_S$  as needed by the inverter, then a discrete  $L_S$  is unnecessary and can be replaced with the WPT coils leakage inductance. Moreover, notice the location of  $L_{mag}$ ,  $C_2$ ,  $Z_{rec}$  and the transformer ratio,  $N$ . As shown in figure 3, a highpass high-low matching network can be formed with  $L_{mag}$ ,  $C_2$ , and  $N$ . If the value of  $L_{mag}$ ,  $C_2$ ,  $Z_{rec}$  and  $N$  are just right, this matching network can be utilized to provide both the impedance matching and filtering needed to connect the rectifier input impedance,  $Z_{rec}$ , to the impedance required by the inverter,  $R_{load}$ . It can be shown that to get the proper matching,  $L_{mag}$  and  $N$  need to satisfy  $L_{mag} = (1/\omega)\sqrt{(R_{load}Z_{rec})/(N^2R_{load} - Z_{rec})}$ . This eliminates the need for discrete filtering and matching inductors and the losses associated with them.

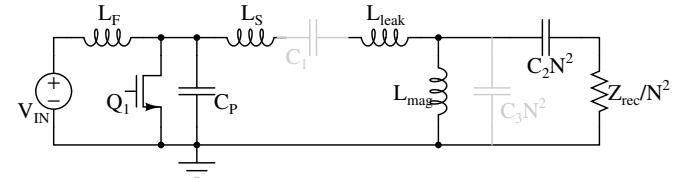


**Fig. 3:** The circuit diagram with all components reflected across the transformer into the inverter side.  $C_1$  and  $C_3$  are colored in gray to assist in the explanation.

While sounding simple, it is practically difficult to design WPT coils to meet all these requirements simultaneously. This is due to the physical constraints of the coils, for example, that the number of turns has to be an integer, that the maximum diameter of the coils is of a certain value, and that the coil separation is fixed, as well as the need to maximize the coupling coefficient between the coils to achieve high transfer efficiency. For the case where WPT coils that meet both of the

aforementioned requirements cannot be found, we can relax the constraints on the leakage inductance, the magnetizing inductance, or both to aid the design process.

1) *Constraint on the  $L_{leak}$*  Instead of designing the WPT coils to have the  $L_{leak}$  value to exactly match the  $L_S$  of the inverter, we allow the leakage inductance to be  $L_{leak} > L_S$ . Then, an extra capacitor,  $C_1$ , can be selected to cancel out the additional inductance, leaving

$$L_{leak} - \frac{1}{\omega^2 C_1} = L_S. \quad (1)$$

2) *Constraint on the  $L_{mag}$*  To facilitate the design process, we relax the constraint on  $L_{mag}$  to  $L_{mag} < (1/\omega)\sqrt{(R_{load}^2 Z_{rec})/(N^2 R_{load} - Z_{rec})}$ . Then, a parallel capacitor  $C_3$  can be used to make its effective inductance at the switching frequency equal to the required value.

$$\frac{L_{mag}}{1 - (\omega^2 L_{mag} C_3 N^2)} = \frac{1}{\omega} \sqrt{\frac{R_{load}^2 Z_{rec}}{N^2 R_{load} - Z_{rec}}} \quad (2)$$

To find the specific coil design that satisfies these relationships, a three-dimensional inductance extraction program such as FastHenry [30] can be used to simulate different WPT coils configuration with different outer diameter, number of turns, turn separation, and coil shapes. For each of the simulated WPT coils, we compare their electrical properties,  $L_{leak}$ ,  $L_{mag}$  and  $N$ , against both the  $L_{leak} > L_S$  and the  $L_{mag} < (1/\omega)\sqrt{(R_{load}^2 Z_{rec})/(N^2 R_{load} - Z_{rec})}$  requirements. Typically, a large number (hundreds to thousands) of simulation is needed to find the best design. Therefore, this process is usually automated via a MATLAB script. Often, many options are available, but the coil configuration with the largest diameter and the smallest number of turns should be used to maximize the coupling coefficient.

Once the suitable WPT coils are identified, we simulate the whole dc-to-dc WPT system with the resonant inductors of the class-E inverter eliminated on LTSpice with the extracted electrical properties of the WPT coils to confirm the operation.

### III. DESIGN EXAMPLE I: RESONANT INDUCTORS ELIMINATION

In this section, a 300 W, 48 V to 48 V, WPT system utilizing the resonant inductors elimination technique as described in section II is demonstrated. This WPT system was originally designed to explore the possibility of replacing the wire connection between the body and the door of a car with a WPT unit. The circuit operates at 13.56 MHz and achieves above 90% dc-to-dc efficiency at 15 mm separation. It consists of a push-pull class-E inverter with its resonant inductors eliminated, WPT coils, and a full-bridge rectifier. To achieve voltage regulation, a hysteresis comparator is used to monitor the output voltage, and to send the on/off signal via an LED/photodiode pair back to the inverter circuit. The detailed design process of this WPT system can be found in [31].

#### A. Inverter & Rectifier Design Summary

As described in section II, in order to design the WPT coils such that their leakage and magnetizing inductance can be utilized as resonant and matching inductor, we must first know the value of  $L_S$ ,  $Z_{rec}$ , and  $R_{load}$ . Thus, the first step in the design process is the design of the inverter and the rectifier (without any inductor eliminated).

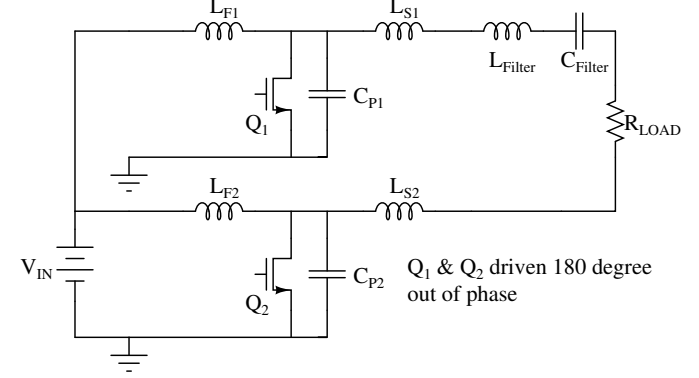


**Fig. 4:** The class-E push-pull topology with two switches  $Q_1$  &  $Q_2$  operating  $180^\circ$  out of phase.

1) *Inverter Design* In order to reduce the input current ripple, a class-E push-pull inverter, shown in figure 4, is used to drive the WPT coils. Figure 5 shows the inverter circuit board, with 650 V 30 A GaN transistors, GS66508T, from GaN Systems used as the main power switches. The inverter is first tested by itself on a resistive RF load. Table I shows the component values and figure 6 shows the estimated loss breakdown of the inverter.

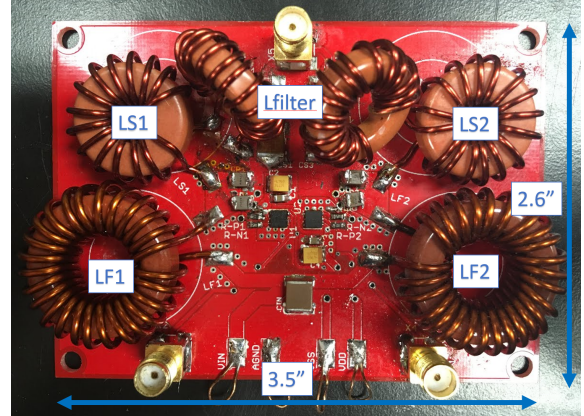


**Fig. 5:** The class E push-pull inverter circuit with all its inductors. Note that the GaN FET is mounted on the underside, and the filter inductor is split into two for symmetry.

**TABLE I:** Operating conditions and passive component values for the push-pull class E inverter.

Frequency [MHz]	$V_{IN}$ [V]	$P_{IN}$ [W]	$L_F$ [nH]	$L_S$ [nH]	$C_P$ [pF]	$L_{Fil}$ [nH]	$C_{Fil}$ [pF]	$R_{load}$ [Ω]
13.56	48	310	1000	110	220	590	230	12.5

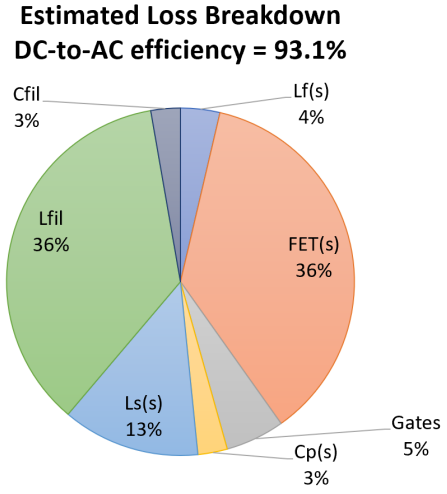


**Fig. 6:** Estimated loss breakdown of the inverter by itself. The dc-to-ac efficiency is the output power at the RF load divided by the dc input power.

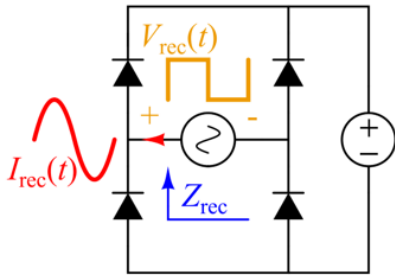


**Fig. 7:** The schematic of a full-bridge rectifier driven with a current source.

2) *Rectifier Design* A full-bridge (FB) passive rectifier, shown in figure 7, is used to rectify the RF power back to dc. In WPT systems where isolation is innate, a FB rectifier is an excellent option due to its simple topology requiring no additional inductors. Here, 60 V 10 A Schottky diodes, PMEG060V100EPD, from Nexperia are used as rectifying diodes. At the desired operating point, the input impedance of this rectifier is,  $Z_{rec} = (8/\pi^2)(V_o^2/P_{out}) = 6.23 \Omega$ . When tested by itself with an RF power amplifier, the efficiency of this FB rectifier is measured to be at 97%.

#### B. WPT Coils Design for Resonant Inductors Elimination

Since the dc-to-ac efficiency of the inverter is 93% and the ac-to-dc efficiency of the rectifier is 97%, if we were to connect the two circuits together with an ideal (lossless) WPT coils and matching network, the maximum dc-to-dc efficiency we can get is 90%. In reality, the matching network and the WPT coils will contribute extra losses, further reducing the dc-to-dc efficiency.

As seen from the loss breakdown of the inverter in figure 6, the majority of the losses outside the transistors occur in the inductors,  $L_S(s)$  and  $L_{fil}$ . If these two components can be eliminated, the overall efficiency will be improved. In this section, the design step used to design the WPT coils such

that their inductances can be used to replace  $L_S(s)$  and  $L_{fil}$  is described.

The design of the WPT coils starts by identifying the largest diameter possible for the particular application requirement. In this case, to effectively replace wired harness connection inside vehicle doors with minimal change to the design of the doors and hinges, the coil has to be less than 70 mm in diameter. At 10s of MHz, standard Litz wire can no longer be used effectively [32], [33]. To achieve high transfer efficiency, thick gauge, solid core, copper wire is used instead. For this prototype, an 8 AWG copper wire is used, although thicker wire can be substituted for higher efficiency.

As outlined in section II, with the value of  $L_S$ ,  $Z_{rec}$ , and  $R_{load}$  previously found, we simulate different coils configurations on FastHenry. For this WPT coils design, we limit the search only to the coils in a spiral configuration for its low profile; however, other arrangements can certainly be used. By varying the outer diameter, the number of turns, and the turn separation, we can create WPT coils with different  $L_{leak}$  and  $L_{mag}$ . A MATLAB script is used to automate this process and to compare the  $L_{leak}$  and  $L_{mag}$  of each simulated WPT coils against the aforementioned constraints:

$$L_{leak} > L_S \quad \text{and}$$

$$L_{mag} < \frac{1}{\omega} \sqrt{(R_{load}^2 Z_{rec}) / (N^2 R_{load} - Z_{rec})}.$$

From the simulation, WPT coils made with two-turn spiral coils both with a 67 mm outer diameter and a 5 mm turn separation placed 15 mm apart pass both of the criteria. Other options are also available, but we select this specific coil configuration for its large diameter and the small number of turn, maximizing the coupling coefficient.

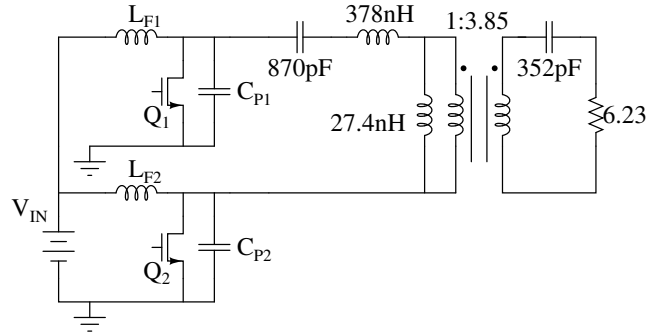


**Fig. 8:** The circuit diagram with the WPT coil shown with all its component values.

With these WPT coils, the lossy inductors in the inverters can now be replaced with  $L_{leak}$  and  $L_{mag}$ . Figure 8 shows these WPT coils in a transformer model along with the values of the capacitors used for the proper matching. Since the  $L_{mag}$  value of these WPT coils is exactly the value needed for the impedance matching, no extra capacitance  $C_3$  is needed. It can be shown that with these values,  $L_{mag}$ ,  $C_2$ , and  $N$  form a perfect resonant matching network, boosting the rectifier

impedance,  $Z_{rec}$ , to the value  $12.5 \Omega$  required by the push-pull inverter. Also, with this specific value of  $C_1$ , part of the  $L_{leak}$  is canceled out at the fundamental frequency, leaving  $L_{leak} - 1/(2\pi f_s)^2 C_1 = 2 \times L_S$  as required by the inverter.

### C. Testing of the WPT System with Resonant Inductors Eliminated

The full system with inductors eliminated is first simulated on LTSpice. Small adjustments on the values of  $C_1$  and  $C_2$  are made to take into account other non-ideality in the design methodology. The final operating condition and passive component values used are shown in table II. Figure 9 shows the final and complete system. Following the inductor elimination technique, only the input inductor  $L_F(s)$  are left on the inverter.

**TABLE II:** Operating conditions and passive component values for the final WPT circuit with inductors eliminated.

Frequency [MHz]	$V_{IN}$ [V]	$V_{OUT}$ [V]	$P_{MAX}$ [W]	$L_F$ [nH]	$C_P$ [pF]	$L_{TX}$ [nH]	$C_1$ [pF]	$L_{RX}$ [nH]	$C_2$ [pF]	$C_{OUT}$ [ $\mu$ F]
13.56	48	48	295	1080	360	374	580	378	375	80

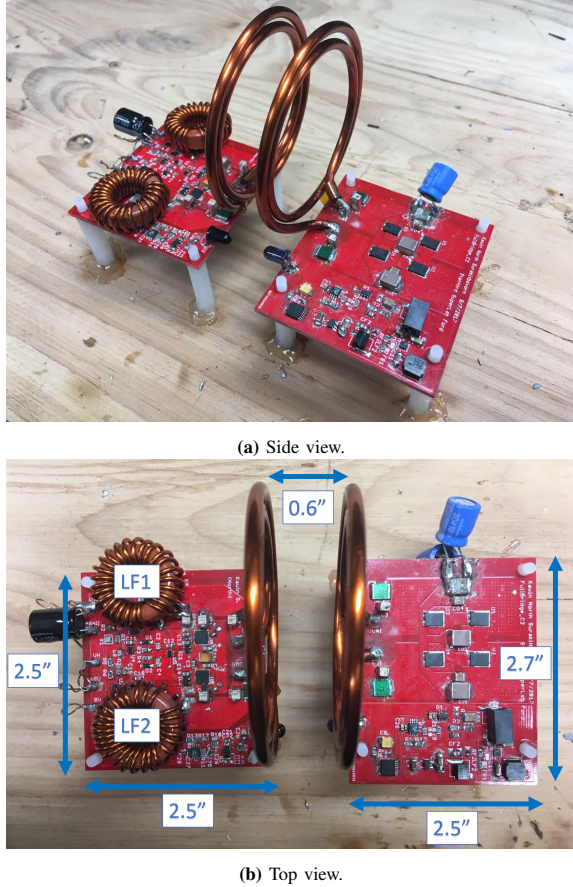


**Fig. 9:** The WPT system with the push-pull class E inverter on the left and the FB rectifier on the right. Notice that both the  $C_1$  and  $C_2$  are split into two for symmetry on the board.

Figure 10 shows the loss percentage breakdown. At full load, the dc-to-dc efficiency of the WPT system, calculated by

dividing the steady-state dc output power at the load resistor by the dc input power from the power supply, is 90.4%. This is equivalent to the efficiency we would get if the inverter circuit without inductors eliminated were to be connected to a rectifier with an ideal loss-less matching network and without the WPT coils. With a simple hysteresis (on/off) controller, the circuit is able to regulate its output voltage and operate efficiently at any load smaller than the maximum load. Figure 11 shows the output voltage at 80% load. Figure 12 shows the first 20 cycles of the drain voltages during the on period. As a result of small  $L_f(s)$ , the drain voltages reach steady state within a few cycles, minimizing the transient loss.

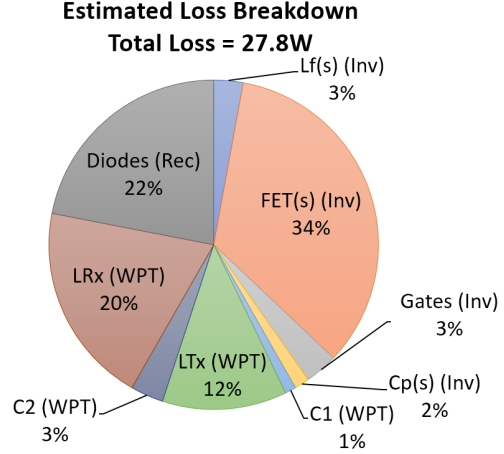


**Fig. 10:** Estimated loss breakdown of the WPT system at full load.



**Fig. 11:** Output voltage at 80% load (teal), drain waveforms (yellow and pink).

## IV. INPUT INDUCTOR ELIMINATION & OPERATING FREQUENCY SELECTION

In this section, a method to eliminate the input inductor from a choke-input class-E inverter circuit will be described. This method relies on the use of the input power supply wires to replace the input inductor. In most applications, these input wires are already part of the system. One downside of this method is the reduced ability to pulse the circuit due to its longer transient. Nonetheless, for specific applications where the weight and size of the system are of a premium, this



**Fig. 12:** The first few cycle of the drain waveforms (yellow and pink) during the on-time.

technique can enable a WPT system design that is extremely low profile and lightweight, as will be shown next in section V.



**Fig. 13:** The twisted pair wires used to demonstrate the input inductor elimination work. (Approx. length = 4 feet 8 inches.)

Figure 13 shows the input power supply wires in the form of twisted pair wires (TPWs) which will be used in the design of section V. The TPWs were 4'8" long and were made from 400-strand 14-AWG wires twisted at roughly nine pitches per foot. We took no special consideration in the selection or making of the wire pair. In order to incorporate these TPWs into the converter design, its impedance is measured and shown in figure 14. In practice, if the material and the construction of the wire pair are precisely known, its impedance characteristic can also be directly calculated. Note that while we use an unshielded TPWs in this paper to demonstrate our input inductor elimination concept, any input wires with sufficient length can be used. This includes but not limited to shielded twisted pair cables, parallel wire cables, and coaxial cables.

Due to their length, these TPWs start to behave like a transmission line past 20 MHz. The first resonant peak of this specific line is at 36 MHz, and the first notch is at 66 MHz. In a previous work by Seo et al. [34] where the input wires were also utilized to eliminate the input inductor, the authors kept their input USB cable looking like a pure inductor by

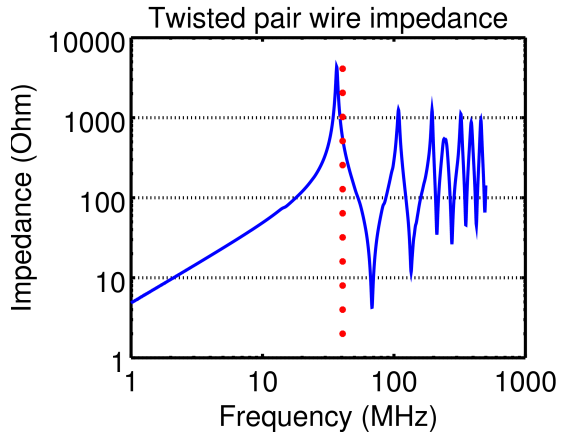


**Fig. 14:** The impedance of the twisted pair wire with one shorted end as measured by an impedance analyzer. The red dotted line represents the 40.68 MHz point.

operating at a frequency well below the first resonant peak of the USB line. While we could certainly design our WPT circuit that way, the lower frequency would mean bigger passive component size in the other part of the system.

Instead, to really miniaturize the circuit, we want to operate at an even higher frequency. For instance, we choose to use the frequency of 40.68 MHz (ISM band) in the design example II with these TPWs. While this TPW resembles a transmission line at this frequency, it can be shown that the class-E operation of the inverter can still be achieved under the conditions that:

1. At the switching frequency, the impedance looking into the TPW,  $Z_{TPW}$ , is much larger than the impedance looking into the drain of the switch,  $Z_{DRAIN}$ .
2. At the second harmonic (twice the switching frequency), the TPW impedance,  $Z_{TPW}$ , is not shorted.

This is in contrast to previous works by Phinney et al. [35], [36] in which transmission lines were utilized at the input of power converters but complicated tuning of the circuit and precise fabrication of the transmission line were required. Since  $Z_{TPW}$  and  $Z_{DRAIN}$  are in parallel, the first condition is set so that the transmission line input will have minimal effect on the overall impedance across the switch at the switching frequency. As for the second requirement, this is set to keep the circuit from going into the regime of a class-Φ inverter [36], which requires a different set of tuning and duty cycle than that of a class-E inverter.

Without this second requirement, if the second harmonics of the switching frequency happened to match the resonant frequency of the transmission line (impedance close to zero), non zero-voltage switching condition will occur across the switch when operating with 50% duty cycle. This can lead to excessive loss and device failure. To prevent this from happening, designer should first measure the impedance of the input line to figure out where the first notch is. For applications where there is no hard limit on what frequency can be used, the switching frequency should be selected so

that its second harmonic is at least 5% apart from this notch. For applications where the switching frequency is limited, i.e., has to be in the ISM-band, the input cable length should be selected/modified such that the same notch-second harmonic separation is achieved. In the extreme case where none of these is possible and the notch of the input cable falls exactly at the second harmonic, a small input inductor (approximately 30 - 50 nH) can be added in series to the input line to slightly shift the impedance toward the lower frequency.

## V. DESIGN EXAMPLE II: INPUT INDUCTOR ELIMINATION

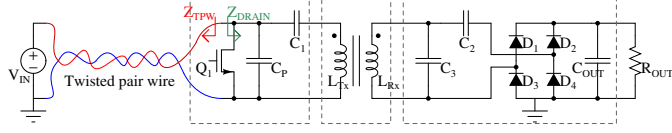


**Fig. 15:** The circuit diagram of the “inductor-less” WPT system.

In this section, the design process of an “inductor-less” 18 V to 18 V proof-of-concept WPT circuit will be described. First, the design process of the WPT unit with input inductor,  $L_F$ , but with resonant inductors eliminated will be described. This circuit is tested to get the baseline performance before the input inductor elimination step. Then, the input TPWs are used to eliminate the input inductor and the circuit performance is again measured. Next, to investigate the reliability of this input elimination method, the circuit is tested against variability in the TPWs length. Finally, the radiated EMI of the input TPWs line of the WPT unit is measured and compared with the baseline case.

**TABLE III:** Operating conditions and design specification for the prototype WPT system.

Frequency [MHz]	$V_{IN}$ [V]	$P_{IN}$ [W]	$P_{OUT}$ [W]	$V_{OUT}$ [V]	Coil sep. [mm]	Coil dia. [mm]
40.68	18	25	20	18	10	30

Table III shows the specification of this system, which is chosen to showcase the design method for its ease of manufacturing and testing. Figure 15 shows the diagram of this WPT unit. The circuit consists of a modified class-E inverter, WPT coils, and a full-bridge rectifier. Unlike a traditional class-E inverter, this modified class-E inverter consists of neither input choke nor output series inductor. The power switch,  $Q_1$  connects directly to the voltage source via a length of twisted pair wires and connects directly to the WPT coils via a series capacitor,  $C_1$ . The WPT coils are represented in the middle by a loosely coupled transformer. The full-bridge rectifier connects to the WPT coils via a parallel and series capacitors,  $C_2$  and  $C_3$ .

### A. Inverter & Rectifier Design Summary

To push the boundary on the frequency of operation, a 100 V 2.7 A EPC8010 GaN HEMT from EPC is used as the main switching device. The design process of the inverter follows the standard class E inverter design as outlined in [37]. Its

component values with all the required inductors,  $L_f$ ,  $L_S$ , and  $L_{fil}$ , are shown in table IV.

**TABLE IV:** Operating condition and component values of the inverter circuit.

Frequency [MHz]	$V_{IN}$ [V]	$P_{IN}$ [W]	$L_f$ [nH]	$L_S$ [nH]	$C_P$ [pF]	$L_{fil}$ [nH]	$C_{fil}$ [pF]	Duty cycle	$R_{load}$ [\Omega]
40.68	18	25	1000	34	90	97	157	0.5	6.7

A full-bridge (FB) passive rectifier is again used to rectify the RF power back to dc. Here, 30 V 2 A Schottky diodes, PMEG3020ER, from Nexperia are used as rectifying diodes. At the desired operating point, the input impedance of this rectifier is,  $Z_{rec} = (8/\pi^2)(V_o^2/P_{out}) = 13.1 \Omega$ .

### B. WPT Coils Design Summary

In this design example, in order to minimize weight and achieve low profile design, flat 2 Oz PCB traces are used to create WPT coils at the expense of transfer efficiency. The WPT coils design follows the same step described previously in section II and III-B. From the simulations, two two-turn spiral coils both with 30 mm outer diameter, 1.5 mm trace width, and 2.5 mm center-to-center turn separation placed 10 mm apart is the best option.

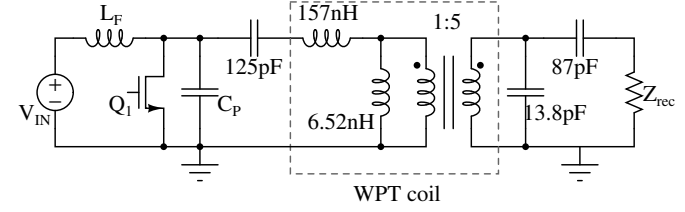


**Fig. 16:** The circuit diagram with the WPT coils shown with all the component values. The self-inductance of each coil is 163 nH, and the coupling coefficient between the coils is 0.2.

Figure 16 shows these WPT coils in a transformer model along with the values of the capacitors as calculated from the equations in section II. With this specific  $C_1$  value, part of  $L_{leak}$  is canceled out at the fundamental frequency, leaving  $L_{leak} - 1/(\omega^2 C_1) = 157 \text{ nH} - 1/((2\pi \times 40.68 \text{ MHz})^2 \times 125 \text{ pF}) = 34 \text{ nH}$  as needed for the class E operation. Furthermore, it can be shown that with these values,  $L_{mag}$ ,  $C_2$ ,  $C_3$  and  $N$  form a perfect resonant matching network boosting the rectifier impedance,  $Z_{rec}$ , to the value of 6.7  $\Omega$  as required by the inverter in section V-A.

### C. Testing of the WPT System before Input Inductor Elimination

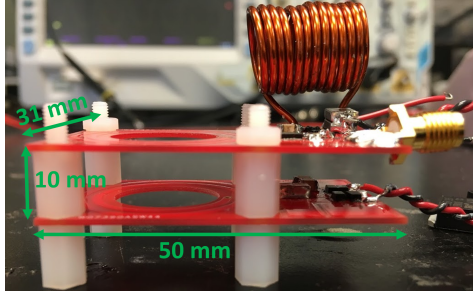
**TABLE V:** Operating conditions and passive component values for the simulated WPT circuit with resonant inductors eliminated.

Freq. [MHz]	$V_{IN}$ [V]	$V_{OUT}$ [V]	$P_{IN}$ [W]	$L_f$ [nH]	$C_P$ [pF]	$L_{TX}$ [nH]	$L_{RX}$ [nH]	$C_1$ [pF]	$C_2$ [pF]	$C_3$ [pF]	$C_{OUT}$ [nF]	$R_{OUT}$ [\Omega]
40.68	18	18	25.3	1000	300	165	165	136	86	45	2	16

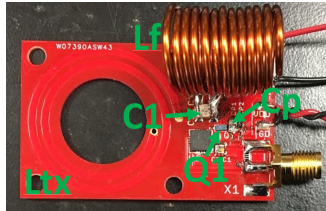
First, the WPT circuit with resonant inductors eliminated is simulated on LTSpice. We made small adjustments to the

component values to take into account non-ideality in the design methodology, parasitic capacitances and inductances in the components, as well as the power losses in the WPT coils. The adjusted operating conditions and passive component values used are shown in table V. According to the simulation, expected dc-to-dc efficiency is approximately 80.5%. Due to the relatively low quality factor of PCB trace inductors, the majority of the loss is expected to be in the WPT coils.

Next, the WPT circuit with resonant inductors eliminated is implemented on the PC boards. As shown in figure 17, the only discrete inductor other than the WPT coils left on the circuit is the  $L_f$ . As expected, even with discrete resonant inductors eliminated, the circuit still maintains ZVS and its characteristic class-E waveform. Nonetheless, the steady state measurement shows the circuit dc-to-dc efficiency, taken from output power at the load on the receiver side divided by the input power from the dc power supply on the transmitter side, to be approximately 72.5%, significantly lower than the simulated value. We believe that this lower efficiency is likely due to the extra losses in the semiconductor devices, and not from the resonant inductors elimination technique. In a paper published in 2017, EPC8010 was explicitly studied [38]. The authors showed that, due to a combination of dynamic on-resistance and  $C_{OSS}$  loss, EPC8010 could exhibit losses 3-4 times higher than the simulated value at 10s of MHz operation. Excessive heating in  $Q_1$  in comparison to other components, shown in figure 18, confirms our hypothesis.



(a) The combined view.



(b) The transmitter side.



(c) The receiver side.

Fig. 17: The WPT circuit with resonant inductors eliminated.

#### D. Input Inductor Elimination via TPWs

The final step in the design of our “inductor-less” WPT system is the elimination of the input inductor. In order to replace  $L_f$  with the input TPWs, we first model the TPW as a series of inductors and capacitors shown in figure 19. After confirming that both of the conditions are met, we simulate the circuit with the input TPW on LTSpice. Small adjustments

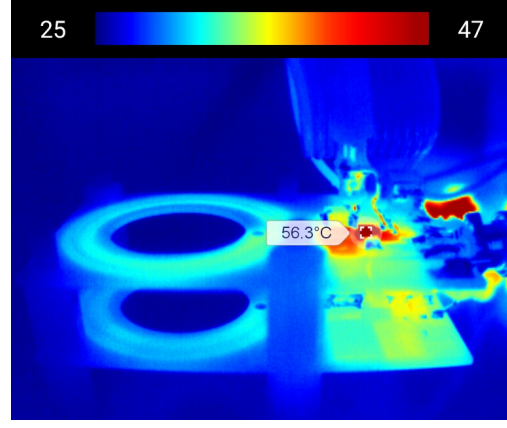


Fig. 18: Thermal image of the WPT circuit tested at 50% pulsed taken after 30 s of operation.

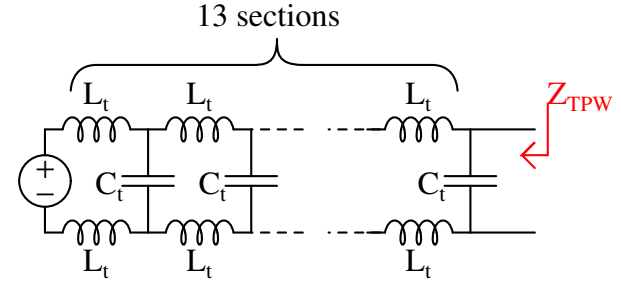


Fig. 19: Transmission line model for the TPW ( $L_t = 40 \text{ nH}$  and  $C_t = 3.8 \text{ pF}$ ).

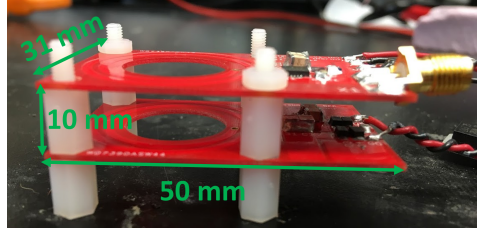
on some of the component values from that of the section V-C are needed to get back zero voltage switching. Nonetheless, the simulated efficiency and the loss breakdown appear the same regardless whether a discrete  $L_f$  or TPWs is used as an input stage.

#### E. Testing of the WPT Circuit with All Discrete Inductors Eliminated (with TPWs Input)

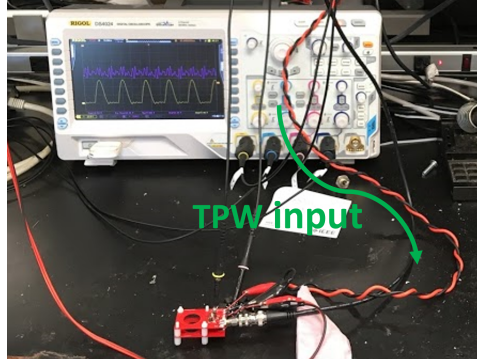
TABLE VI: Operating conditions and passive component values for the tested WPT circuit with all inductors eliminated.

Freq. [MHz]	$V_{IN}$ [V]	$V_{OUT}$ [V]	$P_{IN}$ [W]	$L_f$ [ $\mu\text{H}$ ]	$C_P$ [pF]	$L_{TX}$ [ $\mu\text{H}$ ]	$L_{RX}$ [ $\mu\text{H}$ ]	$C_1$ [ $\mu\text{H}$ ]	$C_2$ [pF]	$C_3$ [pF]	$C_{OUT}$ [nF]	$R_{OUT}$ [ $\Omega$ ]
40.68	18	18.3	28.9	-	210	170	172	122	78	41	2	16

The input inductor,  $L_f$ , along with the input bypass capacitor,  $C_{in}$  are then removed from the circuit, as shown in figure 20. Only small adjustments on the values of  $C_P$  and  $C_1$ , shown in table VI, are needed to achieve a ZVS waveform. Figure 21 shows the drain and output waveform of the circuit. As expected, even with input inductor removed, the circuit can still maintain ZVS and its characteristic class E waveform. The dc-to-dc measurement, taken from the voltage and current at the power supply (pre TPWs) and the voltage and current across the load resistor, shows the circuit efficiency to be at approximately 72%. This is similar to that from the section V-C where the circuit still had a discrete input



(a) The final circuit.



(b) The test setup showing the TPW input.

**Fig. 20:** The final WPT circuit with all discrete inductors eliminated weighting at only 7.5 grams.



**Fig. 21:** Captured drain voltage (yellow) and output voltage (pink) waveform of the WPT circuit with TPW input.

inductor. Furthermore, thermal measurements show the same temperature profile across the boards in both cases confirming that using the TPWs as an input inductor does not lead to a significant increase in the overall losses. Figure 22 shows the estimated loss breakdown of this final circuit.

As can be seen from the loss breakdown, approximately 40% of the loss occurs in the two WPT coils. This loss is disproportionately high due to the use of thin PCB traces as WPT coils. By substituting them with WPT coils made with copper wires, the circuit efficiency can be improved. As for the other 40% of the loss that occurs in the GaNFET, we believe this is due to the combination of dynamic on-resistance and the  $C_{OSS}$  loss in GaN transistors [39], [40]. As the  $C_{OSS}$  loss scales heavily with both the input voltage and the device size, lowering the input voltage and using a device with smaller junction capacitance can further improve the overall efficiency

### Estimated Loss Breakdown DC-to-DC efficiency = 72%

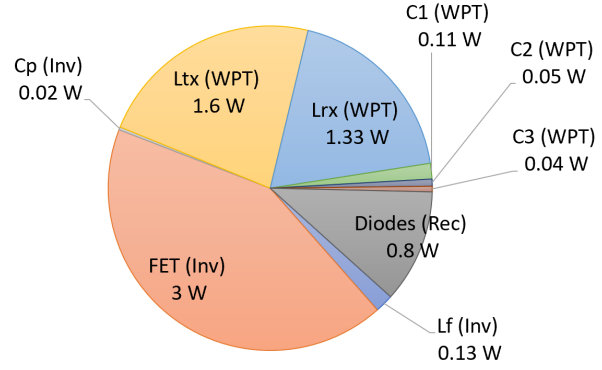


**Fig. 22:** Estimated dc-to-dc efficiency of the final WPT circuit with all discrete inductors eliminated.

[41], [42].

### F. Testing of the “Inductor-less” WPT Circuit with Different TPW Lengths

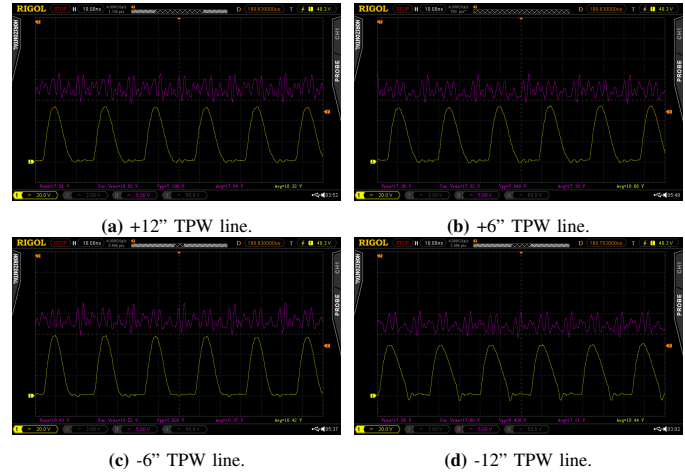


**Fig. 23:** Captured drain voltage (yellow) and output voltage (pink) waveform of the WPT circuit with different TPW input lines.

To demonstrate the circuit's insensitivity to the actual impedance of the TPW transmission line, we perform additional testings with four other TPW lines that are roughly  $\pm 6''$  and  $\pm 12''$  that of the original TPW line. No additional changes in any component values from table VI are done during this testing. Figure 24 shows the measured impedance of the five different TPW lines in comparison to the drain impedance,  $Z_{DRAIN}$ . While the details of their impedances differ, all five lines fit the two criteria mentioned in the section IV. Figure 23 shows the measured drain waveforms across the switch under the varying TPW lengths. While the shapes of the waveforms slightly differ, in all cases, ZVS operations are still achieved. Figure 25 shows the output voltage and the measured efficiency comparison of the proposed WPT circuit when tested with different TPW input lines. Over the tested

range of the input TPW lines, the output voltage varies from 17.3 V to 18.4 V, and the dc-to-dc efficiency varies from 70% to 73%.

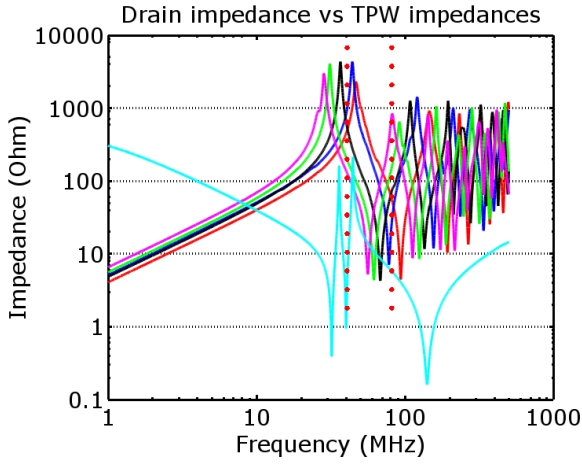


**Fig. 24:** The impedance of the different TPW input lines as measured by an impedance analyzer (pink = +12", green = +6", black = original line, blue = -6", red = -12"), as well as the drain impedance,  $Z_{DRAIN}$ , (cyan). The red dotted lines represent the 40.68 MHz and 81.36 MHz points.

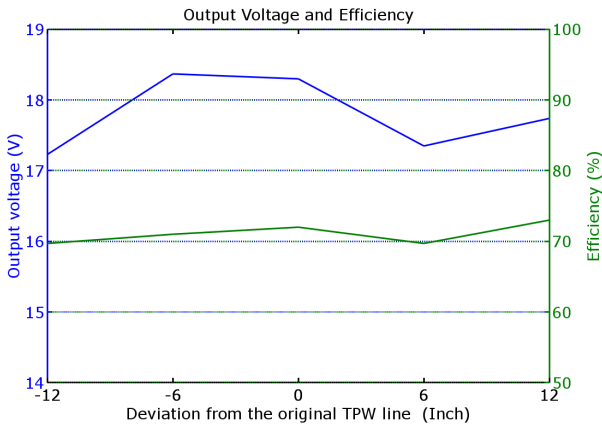


**Fig. 25:** The output voltage and measured dc-to-dc efficiency for the WPT circuit when tested with the different TPW input lines.

#### G. EMI Performance Comparison

To investigate the EMI penalty when the TPWs are used as an input stage instead of a discrete inductor, a simple radiated EMI testing with a near-field probe is performed. A commercial H-field probe, TBPS01-H20 from Tekbox, is used to measure the radiated EMI from the input TPWs. The radiated EMI of three cases are measured: 1. Baseline case with a discrete input inductor (TPWs used as a simple dc power line). 2. TPWs input case (TPWs used as the input stage). 3. Shielded TPWs input case (shown in figure 26 - TPWs wrapped in Aluminum foil with one end of the foil grounded to the power supply ground). In each case, the H-field probe is placed adjacent and pointing to the the TPWs at the point 3 feet down the wire length as measured from

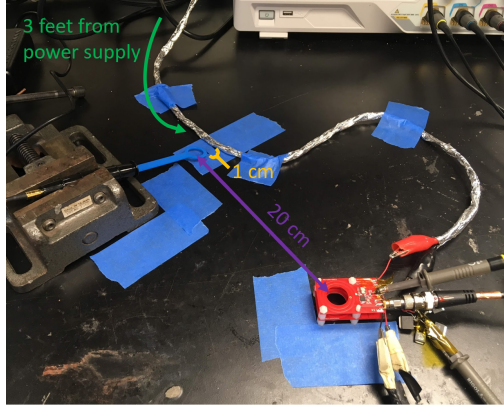


**Fig. 26:** The EMI test setup showing the H-field probe and the shielded TPW input line.

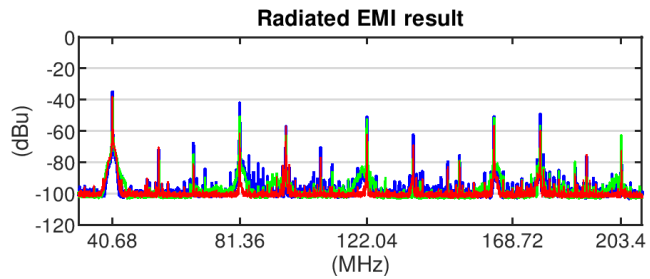


**Fig. 27:** Radiated EMI comparison. Red = case 1 (baseline), blue = case 2 (TPWs input), green = case 3 (shielded TPWs).

the power supply. The distance between the edge of the H-field probe to the edge of the TPWs is 1 cm, and the distance between the H-field probe to the WPT unit is 20 cm.

Figure 27 shows the comparison of the radiated EMI for the three cases. Due to the soft-switching nature of the converter, the EMI profile has narrow peaks mostly around the switching frequency and its harmonics. In all three cases, the radiated EMI at the switching frequency (40.68 MHz) picked up by the H-field probe is comparable with each other. However, the radiated EMI at the first and second harmonic (81.36 MHz and 122.04 MHz) of case 2 and case 3 are significantly higher than that of case 1. We believe that this is due to the TPWs line having lower impedance than that of a discrete inductor at those frequencies allowing harmonics to pass through.

When comparing the shielded TPWs to the unshielded TPWs, EMI reduction at the first harmonics (81.36 MHz) is observed. Nonetheless, the overall EMI reduction from shielding the TPWs line is limited. We believe this is due to the twisting structure of the TPWs already neutralizing most of the emitted EMI from the line.

#### VI. COMPREHENSIVE SUMMARY OF THE PROTOTYPES

In this section, we summarize the key physical attribute, and the electrical performance of each presented prototype. The goal here is to demonstrate the design progression from one prototype to the next, and to highlight the benefits of the inductor elimination technique.

**TABLE VII:** Comprehensive comparison and summary of the prototype in the design example I.

Prototype	Inverter & Rectifier w/o WPT coils before inductors elimination	dc-to-dc WPT system with resonant inductor eliminated
Frequency	13.56 MHz	13.56 MHz
Elec. Specification	48 V to 48 V 300 W	48 V to 48 V 300 W
Num. of Inductors	6	2
Circuit weight	inv: 73 g rec: 20 g	inv: 43 g rec: 20 g
Coils weight	n/a	29.5 g
Coil Dia. & Sep.	n/a	67 mm & 15 mm
Efficiency	dc-to-ac: 93% ac-to-dc: 97%	90.4%

**TABLE VIII:** Comprehensive comparison and summary of the prototype in the design example II.

Prototype	dc-to-dc WPT system with discrete input inductor	dc-to-dc WPT system with TPWs input (sec V-E)	dc-to-dc WPT system with varied length TPWs (sec V-F)
Frequency	40.68 MHz	40.68 MHz	40.68 MHz
Elec. Specification	18 Vdc to 18 Vdc, 25 W	18 Vdc to 18 Vdc 25 W	18 Vdc to 18 Vdc 25 W
Num. of Inductors	1	0	0
Weight	15 g	7.5 g	7.5 g
Box Volume	tx: 38.5 cm <sup>3</sup> rx: 4.65 cm <sup>3</sup>	tx: 4.65 cm <sup>3</sup> rx: 4.65 cm <sup>3</sup>	tx: 4.65 cm <sup>3</sup> rx: 4.65 cm <sup>3</sup>
Coil Dia. & Sep.	30 mm & 10 mm	30 mm & 10 mm	30 mm & 10 mm
Efficiency	72.5%	72%	70 - 73%

\*In all three prototype, resonant inductors elimination technique as described in section VII is used.

### A. Design Example I: Resonant Inductors Elimination

As seen from table VII, by using the inductors elimination technique, we are able to reduce the number of inductors in the system from 6 to 2. This results in both the weight reduction of the circuit, as well as the clear efficiency boost. From our measurement, the WPT coils by themselves has a transfer efficiency (ac-to-ac) of approximately 97%. Had we connected the prototype inverter and rectifier directly to the WPT coils without performing inductor elimination, the resulting dc-to-dc efficiency of the WPT system would have been  $93(\text{inv}) \times 97(\text{rec}) \times 97(\text{wpt}) = 87.5\%$ . Instead, by eliminating the resonant inductors and their associating loss, a higher WPT system dc-to-dc efficiency of 90.4% is achieved.

### B. Design Example II: Input Inductor & Resonant Inductors Elimination

As seen from table VIII, by using the input twisted pair wires as the input stage instead of a discrete inductor, we are able to reduce both the weight and the size of the WPT system significantly. For this prototype, the weight is reduced to 50% and the box volume is reduced to 22%. More importantly, this comes at only a slight to no reduction in the dc-to-dc efficiency when compared with the baseline case where resonant inductors were eliminated but the input choke inductor was still in used.

## VII. CONCLUSION

With the advancement of wide-bandgap devices, WPT systems can be made to operate at an even higher frequency. To achieve ZVS in standard WPT circuits at HF/VHF, multiple discrete inductors are typically needed, making size reduction for low power applications difficult. This paper presents a new way to design a WPT system by absorbing the coils' inductances and use them in other parts of the circuit. The leakage and magnetizing inductance of the WPT coils are

specially designed so they can be used to maintain the ZVS waveform, as well as to perform impedance matching. By designing the WPT coils this way, several unnecessary inductive components can be eliminated. This results in an improvement of the system efficiency, as well as a reduction in the weight and size of the system. With this design method, a high dc-to-dc efficiency of 90.4% at 15 mm separation with 67 mm diameter coil can be achieved. Furthermore, for applications where weight and size are of utmost importance, the switching frequency of the WPT system can also be selected such that the input twisted pair wire can also be utilized to replace the input choke inductor. This results in an extremely small and light-weight circuit. An 18 to 18 V 25 W planar PCB based WPT unit, weighing seven grams, designed with this method is demonstrated. With 10 mm separation and 30 mm coil diameter, a dc-to-dc efficiency of 72% is achieved.

## ACKNOWLEDGMENT

The authors would like to thank Ford Motor Company for their support to the Stanford SUPERLab.

## REFERENCES

- [1] B. Regensburger, A. Kumar, S. Sinha, and K. Afzadi, "High-performance 13.56-mhz large air-gap capacitive wireless power transfer system for electric vehicle charging," in *2018 IEEE 19th Workshop on Control and Modeling for Power Electronics (COMPEL)*, June 2018, pp. 1–4.
- [2] T. Kan, T. Nguyen, J. C. White, R. K. Malhan, and C. C. Mi, "A new integration method for an electric vehicle wireless charging system using lcc compensation topology: Analysis and design," *IEEE Transactions on Power Electronics*, vol. 32, no. 2, pp. 1638–1650, Feb 2017.
- [3] O. C. Onar, J. M. Miller, S. L. Campbell, C. Coomer, C. P. White, and L. E. Seiber, "A novel wireless power transfer for in-motion EV/PHEV charging," in *2013 Twenty-Eighth Annual IEEE Applied Power Electronics Conference and Exposition (APEC)*, March 2013, pp. 3073–3080.
- [4] F. Zhang, S. A. Hackwoth, X. Liu, C. Li, and M. Sun, "Wireless power delivery for wearable sensors and implants in body sensor networks," in *2010 Annual International Conference of the IEEE Engineering in Medicine and Biology*, Aug 2010, pp. 692–695.

- [5] D. Lin, T. Wang, and F. Chen, "Wireless power transfer via rfid technology for wearable device applications," in *2015 IEEE MTT-S 2015 International Microwave Workshop Series on RF and Wireless Technologies for Biomedical and Healthcare Applications (IMWS-BIO)*, Sep. 2015, pp. 210–211.
- [6] S. H. Kang and C. W. Jung, "Wearable and implantable magnetic resonant wireless power transfer," in *2016 URSI Asia-Pacific Radio Science Conference (URSI AP-RASC)*, Aug 2016, pp. 864–866.
- [7] M. Han, J. M. Kim, and H. Sohn, "Dual-mode wireless power transfer module for smartphone application," in *2015 IEEE International Symposium on Antennas and Propagation USNC/URSI National Radio Science Meeting*, July 2015, pp. 111–112.
- [8] A. Abdolkhani, A. P. Hu, M. Moridnejad, and A. Croft, "Wireless charging pad based on travelling magnetic field for portable consumer electronics," in *IECON 2013 - 39th Annual Conference of the IEEE Industrial Electronics Society*, Nov 2013, pp. 1416–1421.
- [9] O. Knecht, R. Bosshard, and J. W. Kolar, "High-efficiency transcutaneous energy transfer for implantable mechanical heart support systems," *IEEE Transactions on Power Electronics*, vol. 30, no. 11, pp. 6221–6236, Nov 2015.
- [10] D. B. Ahire and V. J. Gond, "Wireless power transfer system for biomedical application: A review," in *2017 International Conference on Trends in Electronics and Informatics (ICET)*, May 2017, pp. 135–140.
- [11] S. Stoecklin, T. Volk, A. Yousaf, and L. Reindl, "A programmable and self-adjusting class E amplifier for efficient wireless powering of biomedical implants," in *2015 37th Annual International Conference of the IEEE Engineering in Medicine and Biology Society (EMBC)*, Aug 2015, pp. 3193–3196.
- [12] C. Song, H. Kim, Y. Kim, D. Kim, S. Jeong, Y. Cho, S. Lee, S. Ahn, and J. Kim, "EMI reduction methods in wireless power transfer system for drone electrical charger using tightly coupled three-phase resonant magnetic field," *IEEE Transactions on Industrial Electronics*, vol. 65, no. 9, pp. 6839–6849, Sep. 2018.
- [13] S. Aldhaher, P. D. Mitcheson, J. M. Arteaga, G. Kkelis, and D. C. Yates, "Light-weight wireless power transfer for mid-air charging of drones," in *2017 11th European Conference on Antennas and Propagation (EUCAP)*, March 2017, pp. 336–340.
- [14] J. L. Gomez-Tornero, M. Poveda-García, R. Guzmán-Quijós, and J. C. Sánchez-Arnause, "Design of Ku-band wireless power transfer system to empower light drones," in *2016 IEEE Wireless Power Transfer Conference (WPTC)*, May 2016, pp. 1–4.
- [15] X. Lu, P. Wang, D. Niymato, D. I. Kim, and Z. Han, "Wireless charging technologies: Fundamentals, standards, and network applications," *IEEE Communications Surveys Tutorials*, vol. 18, no. 2, pp. 1413–1452, Secondquarter 2016.
- [16] W. A. Nitz, W. C. Bowman, F. T. Dickens, F. M. Magalhaes, W. Strauss, W. B. Suiter, and N. G. Ziesse, "A new family of resonant rectifier circuits for high frequency dc-dc converter applications," in *APEC '88 Third Annual IEEE Applied Power Electronics Conference and Exposition*, Feb 1988, pp. 12–22.
- [17] A. Majid, J. Saleem, H. B. Kotte, R. Ambatipudi, and K. Bertilsson, "Design and implementation of emi filter for high frequency (mhz) power converters," in *International Symposium on Electromagnetic Compatibility - EMC EUROPE*, Sep. 2012, pp. 1–4.
- [18] A. Majid, J. Saleem, and K. Bertilsson, "Emi filter design for high frequency power converters," in *2012 11th International Conference on Environment and Electrical Engineering*, May 2012, pp. 586–589.
- [19] S. Liu, M. Liu, S. Yang, C. Ma, and X. Zhu, "A novel design methodology for high-efficiency current-mode and voltage-mode class-e power amplifiers in wireless power transfer systems," *IEEE Transactions on Power Electronics*, vol. 32, no. 6, pp. 4514–4523, June 2017.
- [20] M. Fu, T. Zhang, X. Zhu, and C. Ma, "A 13.56 mhz wireless power transfer system without impedance matching networks," in *2013 IEEE Wireless Power Transfer (WPT)*, May 2013, pp. 222–225.
- [21] M. Liu, M. Fu, and C. Ma, "Parameter design for a 6.78-mhz wireless power transfer system based on analytical derivation of class e current-driven rectifier," *IEEE Transactions on Power Electronics*, vol. 31, no. 6, pp. 4280–4291, June 2016.
- [22] M. Fu, H. Yin, M. Liu, and C. Ma, "Loading and power control for a high-efficiency class e pa-driven megahertz wpt system," *IEEE Transactions on Industrial Electronics*, vol. 63, no. 11, pp. 6867–6876, Nov 2016.
- [23] F. Lu, H. Zhang, H. Hofmann, and C. Mi, "A high efficiency 3.3 kw loosely-coupled wireless power transfer system without magnetic material," in *2015 IEEE Energy Conversion Congress and Exposition (ECCE)*, Sep. 2015, pp. 2282–2286.
- [24] R. Matias, B. Cunha, and R. Martins, "Modeling inductive coupling for wireless power transfer to integrated circuits," in *2013 IEEE Wireless Power Transfer (WPT)*, May 2013, pp. 198–201.
- [25] J. Deng, W. Li, T. D. Nguyen, S. Li, and C. C. Mi, "Compact and efficient bipolar coupler for wireless power chargers: Design and analysis," *IEEE Transactions on Power Electronics*, vol. 30, no. 11, pp. 6130–6140, Nov 2015.
- [26] X. Huang and W. Chen, "Wpt topology scheme with dual parallel-circuit class e inverters and integrated inductor," in *2014 International Power Electronics and Application Conference and Exposition*, Nov 2014, pp. 635–638.
- [27] Z. N. Low, R. A. Chinga, R. Tseng, and J. Lin, "Design and test of a high-power high-efficiency loosely coupled planar wireless power transfer system," *IEEE Transactions on Industrial Electronics*, vol. 56, no. 5, pp. 1801–1812, May 2009.
- [28] M. K. Uddin, G. Ramasamy, S. Mekhilef, K. Ramar, and Y. C. Lau, "A review on high frequency resonant inverter technologies for wireless power transfer using magnetic resonance coupling," in *2014 IEEE Conference on Energy Conversion (CENCON)*, Oct 2014, pp. 412–417.
- [29] A. P. Sample, D. T. Meyer, and J. R. Smith, "Analysis, experimental results, and range adaptation of magnetically coupled resonators for wireless power transfer," *IEEE Transactions on Industrial Electronics*, vol. 58, no. 2, pp. 544–554, Feb 2011.
- [30] M. Kamon, M. J. Tsuk, and J. K. White, "FASTHENRY: a multipole-accelerated 3-D inductance extraction program," *IEEE Transactions on Microwave Theory and Techniques*, vol. 42, no. 9, pp. 1750–1758, Sept 1994.
- [31] K. Surakitbovorn and J. Rivas-Davila, "Design of a GaN-based wireless power transfer system at 13.56 MHz to replace conventional wired connection in a vehicle," in *2018 International Power Electronics Conference (IPEC-Niigata 2018 -ECCE Asia)*, May 2018, pp. 3848–3854.
- [32] C. R. Sullivan, "Layered foil as an alternative to litz wire: Multiple methods for equal current sharing among layers," in *2014 IEEE 15th Workshop on Control and Modeling for Power Electronics (COMPEL)*, June 2014, pp. 1–7.
- [33] B. A. Reese and C. R. Sullivan, "Litz wire in the MHz range: Modeling and improved designs," in *2017 IEEE 18th Workshop on Control and Modeling for Power Electronics (COMPEL)*, July 2017, pp. 1–8.
- [34] G. S. Seo and H. P. Le, "An inductor-less hybrid step-down DC-DC converter architecture for future smart power cable," in *2017 IEEE Applied Power Electronics Conference and Exposition (APEC)*, March 2017, pp. 247–253.
- [35] J. Phinney, J. H. Lang, and D. J. Perreault, "Multi-resonant microfabricated inductors and transformers," in *2004 IEEE 35th Annual Power Electronics Specialists Conference (IEEE Cat. No.04CH37551)*, vol. 6, June 2004, pp. 4527–4536 Vol.6.
- [36] J. W. Phinney, D. J. Perreault, and J. H. Lang, "Radio-frequency inverters with transmission-line input networks," in *2006 37th IEEE Power Electronics Specialists Conference*, June 2006, pp. 1–9.
- [37] N. O. Sokal and A. D. Sokal, "Class E-A new class of high-efficiency tuned single-ended switching power amplifiers," *IEEE Journal of Solid-State Circuits*, vol. 10, no. 3, pp. 168–176, Jun 1975.
- [38] K. Surakitbovorn and J. R. Davila, "Evaluation of GaN transistor losses at MHz frequencies in soft switching converters," in *2017 IEEE 18th Workshop on Control and Modeling for Power Electronics (COMPEL)*, July 2017, pp. 1–6.
- [39] B. Lu, T. Palacios, D. Risbud, S. Bahl, and D. I. Anderson, "Extraction of dynamic on-resistance in GaN transistors: Under soft- and hard-switching conditions," in *2011 IEEE Compound Semiconductor Integrated Circuit Symposium (CSICS)*, Oct 2011, pp. 1–4.
- [40] G. Zulauf, S. Park, W. Liang, K. Surakitbovorn, and J. M. R. Davila, " $C_{OSS}$  losses in 600 V GaN power semiconductors in soft-switched, high- and very-high-frequency power converters," *IEEE Transactions on Power Electronics*, vol. PP, no. 99, pp. 1–1, 2018.
- [41] K. Surakitbovorn, L. Gu, and J. Rivas-Davila, "On the optimal input voltage of a class-e power amplifier with gan hemts at mhz frequency operation," in *2019 20th Workshop on Control and Modeling for Power Electronics (COMPEL)*, June 2019, pp. 1–8.
- [42] K. Surakitbovorn and J. M. Rivas-Davila, "On the optimization of a class-e power amplifier with gan hemts at mhz operation," *IEEE Transactions on Power Electronics*, pp. 1–1, 2019.